Published in final edited form as:
Proc SPIE. 2008 April 18; 6913: 691342–. doi:10.1117/12.772303.

A dual micro-CT system for small animal imaging

C.T. Badea, **S. Johnston**, **B. Johnson**, **M. Lin**, **L.W. Hedlund**, and **G. Allan Johnson**
Center for In Vivo Microscopy, Dept. of Radiology, Duke University Medical Center, Durham, NC 27710

Abstract

Micro-CT is a non-invasive imaging modality usually used to assess morphology in small animals. In our previous work, we have demonstrated that functional micro-CT imaging is also possible. This paper describes a dual micro-CT system with two fixed x-ray/detectors developed to address such challenging tasks as cardiac or perfusion studies in small animals. A two-tube/detector system ensures simultaneous acquisition of two projections, thus reducing scanning time and the number of contrast injections in perfusion studies by a factor of two. The system is integrated with software developed in-house for cardio-respiratory monitoring and gating. The sampling geometry was optimized for 88 microns in such a way that the geometric blur of the focal spot matches the Nyquist sample at the detector. A geometric calibration procedure allows one to combine projection data from the two chains into a single reconstructed volume. Image quality was measured in terms of spatial resolution, uniformity, noise, and linearity. The modulation transfer function (MTF) at 10% is 3.4 lp/mm for single detector reconstructions and 2.3 lp/mm for dual tube/detector reconstructions. We attribute this loss in spatial resolution to the compounding of slight errors in the separate single chain calibrations. The dual micro-CT system is currently used in studies for morphological and functional imaging of both rats and mice.

Keywords

Micro-CT; cardiac imaging; calibration; small animal

1. INTRODUCTION

The dual micro-CT system described here is designed to address the challenges associated with functional imaging studies in small animals, such as in cardiopulmonary or perfusion applications. For such demanding applications, e.g. cardiac studies in a mouse, both high temporal (10 ms) and spatial resolutions (100 microns) are necessary[1]. We have achieved this performance with our previous prototype single x-ray tube/detector system using prospective cardio-respiratory gating strategies[2]. We have used cine micro-CT for anatomical and functional phentoyping of transgenic mice[3], and to assess in vivo the size of myocardial infarction, as well as the cardiac function in infarcted mice[4]. In addition, we have used a combined micro-CT and digital subtraction angiography (DSA) approach to image both morphology and perfusion in tumors[5]. However, one of the problems associated with our single-chain system is the longer time (5–10 minutes) required for sampling of a dataset. The dual system addresses this limitation by reducing the sampling time by half.

2. METHODS

The mouse is 4000-times smaller than a human and its heart beats 10-times faster. To compensate for such differences from mouse to human, we designed and built our first generation micro-CT system[2] using an x-ray tube able to deliver very high fluence rates

with very short exposure times (10 ms). Therefore, projection images with good signal-to-noise-ratios and no motion blurring are possible. For the present dual micro-CT system (see Fig. 1), we used two Varian A197 (Salt Lake City, UT) x-ray tubes with dual focal spots fs=0.6/1 mm. The tubes are designed for angiographic studies with high instantaneous flux and total heat capacity. Two Epsilon high-frequency x-ray generators produced by EMD Technologies (Quebec, Canada) are used to control both x-ray tubes. The system has two identical detectors with a Gd_2O_2S phosphor (XDI-VHR 2 Photonic Science, East Sussex, UK) with pixels of 22 microns, 110 mm input taper size, and 4008 × 2672 image matrix. Both detectors allow on-chip binning of up to 8 × 8 pixels, and sub-area readout to allow higher speed readout of 10 frames/sec, i.e. a time resolution of 100 ms. Both tubes and detectors are mounted on a table together with the rotation stage. The vertically positioned animal is placed in a cradle that is rotated via an Oriel Model 13049 digital stepping motor. The x-ray generators, tubes, detectors, and the rotation are controlled by a Sequencer application written in LabVIEW (National Instruments, Austin, TX) that allows cardio-respiratory gating strategies.

2.1 Sampling geometry

The sampling geometry was optimized in such a way that the geometric blur of the focal spot matches the Nyquist sample at the detector as described in[2].

We consider scanning a rat of a maximum diameter S =70.0 mm placed at an Object Detector Distance ODD=100.0 mm. The computations for optimum system geometry are based on the requirements of high instantaneous flux, a reconstruction with a 44 or 88-micron voxel size and reduced cone angle.

ODD=100.0 mm ensures a rather conservative distance between rat and detector (65 mm). With this ODD value, the rat central axis is projected in the center of both detectors (Photonic Science X-RAY VHR 2 tap with diameter of 110 mm, active area =90×60 mm). We use x-ray tubes with dual focal spots, i.e. *fs*=0.6/1 mm. The penumbra blurring is given by eq. 1:

$$SDD = ODD + fs^{*} ODD / b; \tag{1}$$

where SDD refers to the source to detector distance and *b* is the penumbra blurring.

The flux is related to the *fs* and *SDD* by eq. (2):

$$\varphi \propto \frac{fs^{1.5}}{SDD^{2}} \tag{2}$$

If one sets the *SDD* so the penumbral blur (*b*) of a given focal spot is equal to the Nyquist sample defined by the detector spacing (*res*), one can solve for the flux as a function of the resolution (eq. 3).

$$\varphi \propto \frac{fs^{1.5}}{\left(\frac{fs * ODD}{res} + ODD\right)^{2}} \tag{3}$$

For focal spot *fs*=0.6 mm, the SDD values for the resolutions of 44 and 88 microns are 1464 mm and 781 mm, respectively. An SDD=781 mm corresponding to 88-micron resolution

offers also the highest achievable photon fluence for the two available focal spots (see Fig. 2). For the focal spot *fs*= 1 mm, and for the corresponding resolutions of 44 and 88 microns, the SDD values are 2373 mm and 1236 mm, respectively. We note that the first distance (SDD =2373 mm) is not practical with our system, since it is larger than the dual micro-CT table dimension of 1600 mm. In the case of cone beam CT reconstruction using Feldkmap algorithm[6], it is also important for the cone angle to be less than 10° to minimize artifacts. The cone angle is less than 10° for SDD >180 mm, and therefore it was a not a limitation for the present system.

Our choice for scanning with the present system has been the geometry for reconstruction at 88 microns (where the available flux is maximum) and having values for SDD around 781mm and for ODD around 100mm. While these tubes/detectors and rotation stages were positioned to match these distances, their accurate values used in the reconstruction process were given by the geometric calibration procedure.

2.2 Geometric calibration

An important requirement for successful dual micro-CT imaging is to combine projections from the two chains in a single reconstruction process. This involves a geometric calibration procedure presented in[7]. In essence, the geometric calibration is achieved by scanning a calibration phantom with metallic beads and computing the projections matrices required by the reconstruction. The individual geometries of the imaging chains were estimated from the phantom projection images using analytical methods similar to[8], followed by a refinement procedure based on non-linear optimization. The geometric parameters were used to create the cone beam projection matrices required by the reconstruction process for each imaging chain. Next, a transformation between the two projection matrices was found that allowed the combination of projection data of the two imaging chains, in a single reconstructed image. To visually verify the geometric calibration for the dual micro-CT system, we performed an experiment where a dead C57BL mouse was scanned and we compared the image quality of reconstruction using data acquired with single tube and dual tube micro-CT.

2.3 Image acquisition and reconstruction

Due to the two orthogonal imaging chains, projections for at least 180° are obtained by rotating the mouse over a circular orbit of approximately 90°. Similar to the fan angle case for Feldkamp reconstruction, it is required to have projections in a 180° + fan angle. For most of our experiments with our dual micro-CT, one chain is acquiring projections for an arc (−91.5°, 0°), while the second imaging chain is acquiring projections for the arc corresponding to (0°, 95°). A representation of how these projections are radially positioned based on the central slice theorem[9] is shown by Fig. 3. This representation is a simplification, since our sampling geometry is actually cone beam. However, due to the long SDD and comparable SOD, the system presented here is close to a 3D parallel beam cases and therefore, we considered this as an adequate representation (see Fig. 3). The sampling is performed at 80kVp, 160mA, and 10 ms per exposure. The number of projections acquired depends on the experiment, but is generally around 380. The projections and the projection matrices are used with the Cobra EXXIM software package (EXXIM Computing Corp., Livermore, CA) to reconstruct tomographic data as 3D image arrays (512^3).

2.4 Cardio-respiratory gating

For our in vivo experiments, animals are intubated and mechanically ventilated to allow scan synchronous ventilation, i.e., the imaging is triggered only during end-expiration. In previous work, we described a prospective gating approach regarding cardiac motion[1]. In that work, the acquisition of each projection was triggered when the predefined phase of the

cardiac cycle (systole or diastole) occurred in a predefined window during end-expiration. The same approach is implemented with the present dual micro-CT system. We have also implemented a retrospective approach for cardiac gating, where projections are acquired during end-expiration, but at randomly occurring phases of the cardiac cycle and sorted retrospectively based on the recorded ECG signal in projections sets corresponding to each cardiac phase[10].

2.5 Experimental evaluation

2.5.1 Uniformity and noise—The uniformity of signal response of the present system was studied by imaging a cylindrical water phantom (3 cm in diameter), covering the size of an average mouse. To compare the variation across the field of view, the radial profile through the center of the water cylinder was examined. On the central slice, signal intensity and standard deviation were measured in a 3×3×3 mm^3 region of interest (ROI) at the center of the cylinder, as well as in four similar ROIs at the periphery. We also measured the noise level in and its dependency on the number of projections i.e. for (760, 380, 254, 190) projections.

2.5.2 Linearity—The linearity phantom consisted of 5 ml vials, filled with either water or with varying iodine concentrations covering the range of signal intensities seen in contrast-enhanced animal experiments. Iodine concentrations of (2.5, 5, 10, 20, 30, 0) mg iodine per ml were prepared in the lab from non-ionic iohexal contrast material (Isovue 370 Bracco Diagnostics). The signal intensity was measured for each iodine concentration in a 3×3×3 mm^3 ROI in the center of each vial. Linear regression was performed as signal intensity was plotted as a function of increasing iodine concentration.

2.5.3 MTF measurements—In order to assess the resolution performance of the new dual micro-CT system, we scanned a cylindrical phantom to assess the modulation transfer functions (MTFs), as described in American Society for Testing and Materials (ASTM)[11]. We computed the MTF for both single and dual-chain reconstructions. We know that imperfect calibration would cause double contours and blur the reconstructed images. Therefore, we also used the MTFs as a more quantitative figure of merit to assess the performance of the calibration.

2.5.4 Dose—A major limitation of micro-CT imaging is the effect of ionizing radiation, which can lead to immediate radiation damage and long-term genetic damage. This becomes especially important when considering longitudinal studies that require repeated exposures to the same animal. The LD50/30 for a mouse is reported to be approximately 700 cGy[12]. Dose was measured using a Wireless Dosimetry System Mobile MOSFET TN-RD-16, SN 63 (Thomson/Nielsen, Ottawa, ON, Canada). Five MOSFET dosimeters having silicon chips of $1mm^2$ and an active area 0.2mm x 0.2mm were positioned at the surface and the center of a rodent-like phantom made out of acrylic.

2.6 Animal experiments

In vivo experiments were performed in mice and rats following protocols approved by the Duke Institutional Animal Care and Use Committee. To show the cardio-respiratory gating capabilities of our system, we imaged Fischer 344 rats (National Cancer Institute, Frederick Cancer Center) with an average weight of 140 g. Animals were anesthetized with a 50 mg/kg intra-peritoneal injection of sodium pentobarbital and 2 mg/kg butorphanol. An endotracheal tube was inserted perorally and a tail vein was catheterized for contrast injection. During imaging, anesthesia was maintained with 2–3% isoflurane (Halocarbon, River Edge, NJ) delivered by a custom-made mechanical ventilator (80 breaths/min)[13]. For imaging, the animal was positioned in an acrylic cradle held in the vertical position by a bar

behind the upper incisor with paws taped to the sides of the cradle. The bottom end of the cradle was placed in a pedestal rotated by a computer-controlled stepping motor. Temperature was maintained using an infrared lamp and a temperature controller. Prior to imaging, iodinated liposome contrast agent was infused via tail vein catheter (0.012 ml/kg). The blood pool contrast agent contained 100 mgI/ml and is described in detail by Mukundan and colleagues[14]. Projection images were acquired using a prospective gating approach in systole and diastole based on the ECG signal. The time required sampling the systole and diastole datasets was approximately 5 mins.

3. RESULTS

As shown by Fig. 4C for a reconstructed voxel of 88^3 microns, the average level of noise (standard deviation of the reconstructed values in ROI) was about 75 HU, with a radiation dose of 0.095Gy when 380 projections were used. The noise level can be reduced to 57 HU if the number of projections is doubled. The system has a linear response (see Fig. 5). A strong linear correlation exists between the enhancement (CT number) and the increasing iodine concentration. Ring artifacts currently limit the image quality (see Fig 5A). Further work is under way to reduce these circular ring artifacts.

Fig. 6(A, B) displays micro-CT images of slices in sagittal orientation of the dead mouse head using the single and dual tube/detector micro-CT reconstructions. This particular anatomic location presents a particularly good test for the high-frequency components arising from the detailed bony structures in the jaws. Although projections from both imaging chains were used in the reconstruction of the dual tube/detector micro-CT images, they show no obvious misalignments artifacts and the image quality of single and dual chain micro-CT are comparable, visual proof that the calibration method performed well. Fig. 6C presents the MTF plots for the single and dual tube/detector reconstructions.

The MTF at 10% is 3.4 lp/mm for single detector reconstructions, and 2.3 lp/mm for dual tube/detector reconstructions. We attribute this loss in spatial resolution from single to dual micro-CT to the compounding of slight errors in the separate single chain calibrations.

Examples of cardiac micro-CT images acquired during diastole and systole in rat are shown by Fig. 7. The contrast difference between the myocardium and blood in the left ventricle was approximately 250 HU. No blurring artifacts are present around the heart or the diaphragm, which confirmed that the gated acquisition was working properly.

4. DISCUSSIONS AND CONCLUSIONS

This paper describes a unique dual chain micro-CT system designed for both morphological and functional imaging in small animals. We demonstrate here that we can successfully reconstruct 3D volume images by combining data from the two imaging chain in a single reconstruction free of misalignment artifacts (see Figs. 6, 7) using our recently developed geometric calibration procedure[7]. Using multiple imaging chains opens up an interesting array of possibilities for novel imaging methods. In this current work, we have used the system with object rotations of around 90°. But other sampling strategies are possible where, for example, the object would be rotated around 180° and the projections acquired by the two tubes would be interleaved. In fact, the angle between the two chains can be varied around 90° and could become an interesting parameter to change for investigation of other projection sampling strategies, particularly for 4D functional assessment. Another interesting area for our future developments will be on gating strategies. The dual micro-CT system and the sampling strategies based on retrospective gating will allow us in the future to reduce the data acquisition times for cardiac or perfusion studies. Indeed, sampling using

a retrospective approach is more efficient, but it will also require other reconstruction approaches that could better deal with irregular angular distribution and limited number of projections. Such a reconstruction algorithm based on total variation was recently described and will be used with our future studies [10].

Much of our 4D imaging to date has focused on cardiac function. But perfusion imaging is another area where the dual imaging chain will be of significant benefit. As shown recently, perfusion studies can be done in small animals using tomographic digital subtraction angiography (DSA)[15] and a dual system will allow increased data collection and/or a reduction the number of contrast agent injections.

Dual energy CT with the associated benefits on contrast resolution and material differentiation[16] is yet another area where the dual imaging chain can be used to great benefit.

Two final attributes of the system described here are the open architecture and modular structure of the system. The workbench on which the detectors and x-ray sources have been assembled can readily accommodate other complementary imaging methods. For example, adding a stationary SPECT camera will be quite straightforward. The existing animal support and system control software can provide triggers to synchronize acquisition of projection data at systole/diastole, etc. Data will be inherently registered with the anatomic data from the CT acquisition. Optical imaging chains can be readily envisioned as well, where addition of other sources and detectors (e.g. near infrared) can be accomplished with virtually no modification to the existing platform. We envision this system as a fundamental building block—a Molecular Imaging Workbench, to provide structure for a number of exciting multimodality imaging systems.

In conclusion, this paper presents our successful implementation of the dual micro-CT system and results for cardiac imaging in rodents. The system is flexible and amenable to integration with other modalities, such as such fluorescence optical tomography, laying the basis for a whole new generation of small animal imaging systems.

Acknowledgments

This work was performed at the Duke Center for In Vivo Microscopy, an NIH/NCRR National Biomedical Technology Resource Center (P41 RR005959) and NCI Small Animal Imaging Resource Program (U24 CA092656), and was also supported by NCI (R21 CA124584-01).

References

1. Badea C, Fubara B, Hedlund L, Johnson GA. 4D micro-CT of the mouse heart. Mol Imaging. 2005; 4(2):110–116. [PubMed: 16105509]
2. Badea CT, Hedlund LW, Johnson GA. Micro-CT with respiratory and cardiac gating. Med Phys. 2004; 31 (12):3324–3329. [PubMed: 15651615]
3. Badea CT, Hedlund LW, Mackel JF, Mao L, Rockman HA, Johnson GA. Cardiac microcomputed tomography for morphological and functional phenotyping of muscle lim protein null mice. Mol Imaging. 2007; 6 (4):261–268. [PubMed: 17711781]
4. Nahrendorf M, Badea C, Hedlund LW, Figueiredo JL, Sosnovik DE, Johnson GA, Weissleder R. High-resolution imaging of murine myocardial infarction with delayed-enhancement cine micro-CT. Am J Physiol. 2007; 292 (6):H3172–3178.
5. Badea CT, Hedlund LW, Lin MD, Boslego JF, Johnson GA. Tumor imaging in small animals with a combined micro-CT/micro-DSA system using iodinated conventional and blood pool contrast agents. Contrast Media and Molecular Imaging. 2006; 1:153–164. [PubMed: 17193692]

6. Feldkamp LA, Davis LC, Kress JW. Practical cone-beam algorithm. J Opt Soc Am. 1984; 1 (6): 612–619.
7. Johnston S, Johnson GA, Badea C. Geometric calibration for a dual tube/detector micro-CT system. Med Phys. 2007 submitted.
8. Yang K, Kwan AL, Miller DF, Boone JM. A geometric calibration method for cone beam CT systems. Med Phys. 2006; 33 (6):1695–1706. [PubMed: 16872077]
9. Kak, CA.; Slaney, M. Principles of computerized tomographic imaging. IEEE Press; New York: 1988. p. 327
10. Song J, Liu QH, Johnson GA, Badea CT. Sparseness prior based iterative image reconstruction for retrospectively gated cardiac micro-CT. Med Phys. 2007; 34 (11):4476–4483. [PubMed: 18072512]
11. American Society for Testing and Materials (ASTM). Standard test method for measurements of computed tomography (CT) system performance. Philadelphia: 1995.
12. Ford NL, Thornton MM, Holdsworth DW. Fundamental image quality limits for microcomputed tomography in small animals. Med Phys. 2003; 30:2869–2877. [PubMed: 14655933]
13. Hedlund LW, Johnson GA. Mechanical ventilation for imaging the small animal lung. ILAR J. 2002; 43(3):159–174. [PubMed: 12105383]
14. Mukundan S, Ghaghada K, Badea C, Hedlund L, Johnson G, Provenzale J, Bellamkonda R, Annapragada A. A nanoscale, liposomal contrast agent for preclincal microCT imaging of the mouse. Am J Roentgenology. 2006; 186:300–307.
15. Badea CT, Hedlund LW, De Lin M, Mackel JS, Samei E, Johnson GA. Tomographic digital subtraction angiography for lung perfusion estimation in rodents. Med Phys. 2007; 34 (5):1546–1555. [PubMed: 17555236]
16. Johnson TR, Krauss B, Sedlmair M, Grasruck M, Bruder H, Morhard D, Fink C, Weckbach S, Lenhard M, Schmidt B, Flohr T, Reiser MF, Becker CR. Material differentiation by dual energy CT: initial experience. Eur Radiol. 2007; 17 (6):1510–1517. [PubMed: 17151859]

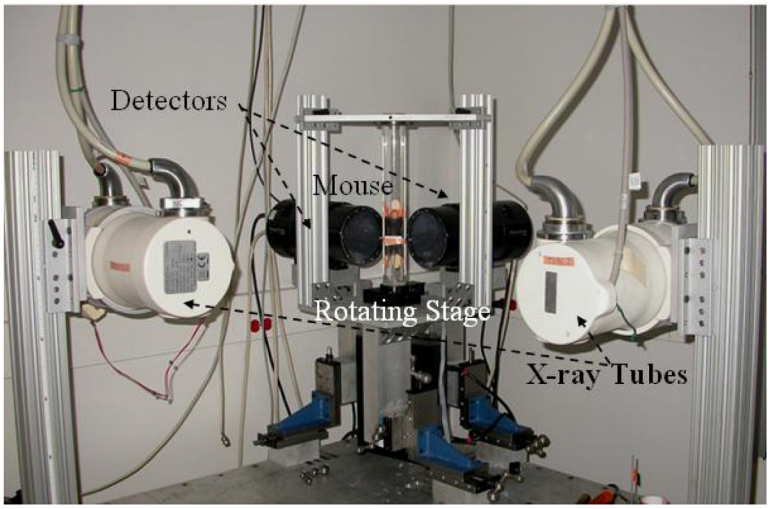

Fig. 1.
The dual micro-CT system uses rotating platform geometry. The x-ray tubes and the detectors are arranged orthogonally. The sampling is controlled by a Sequencer application written in LabVIEW.

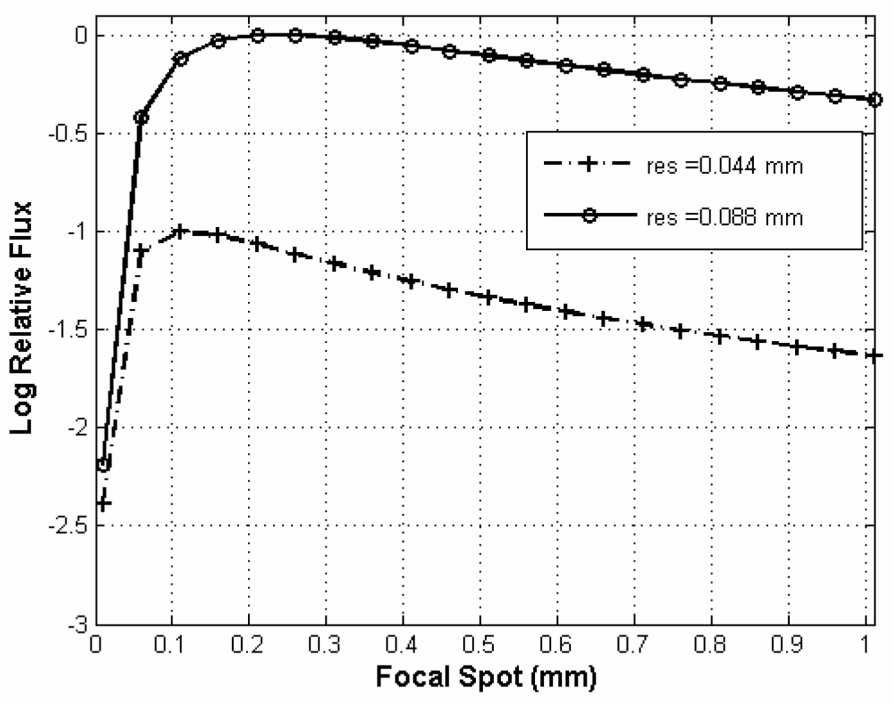

Fig. 2.

Relative fluence rate is plotted as a function of focal spot dimension for limiting resolution at 44 and 88 microns. The fluence rate is normalized to the maximum that is attained for resolution at 88 microns with a focal spot of 0.21 mm.

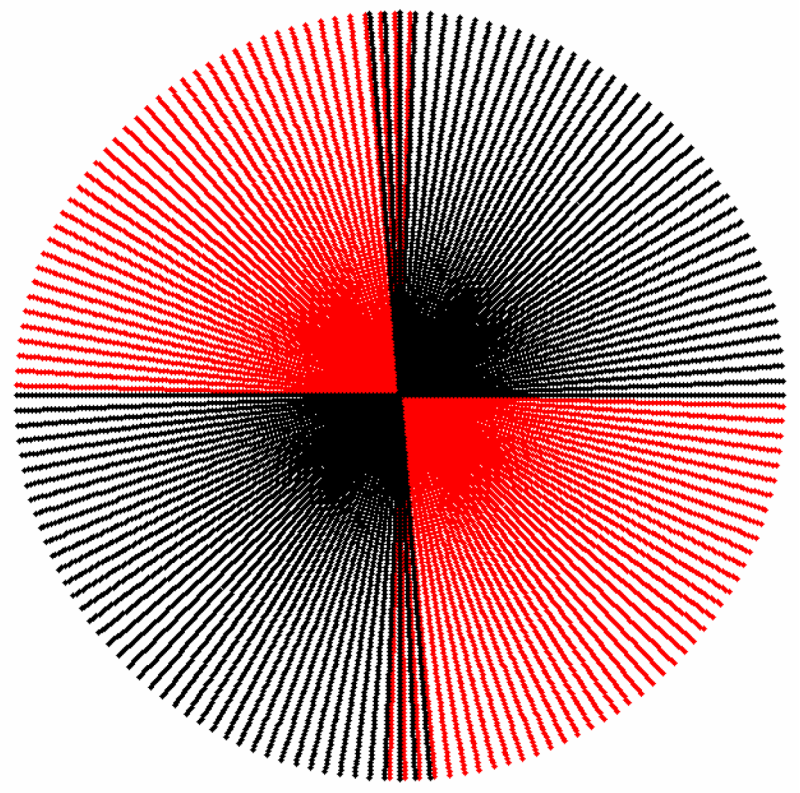

Fig. 3.
The radial disposition of projections for one chain (red) covering the (−91.5°, 0°), while the second imaging chain is acquiring projections for the arc corresponding to (0°, 95°) (black).

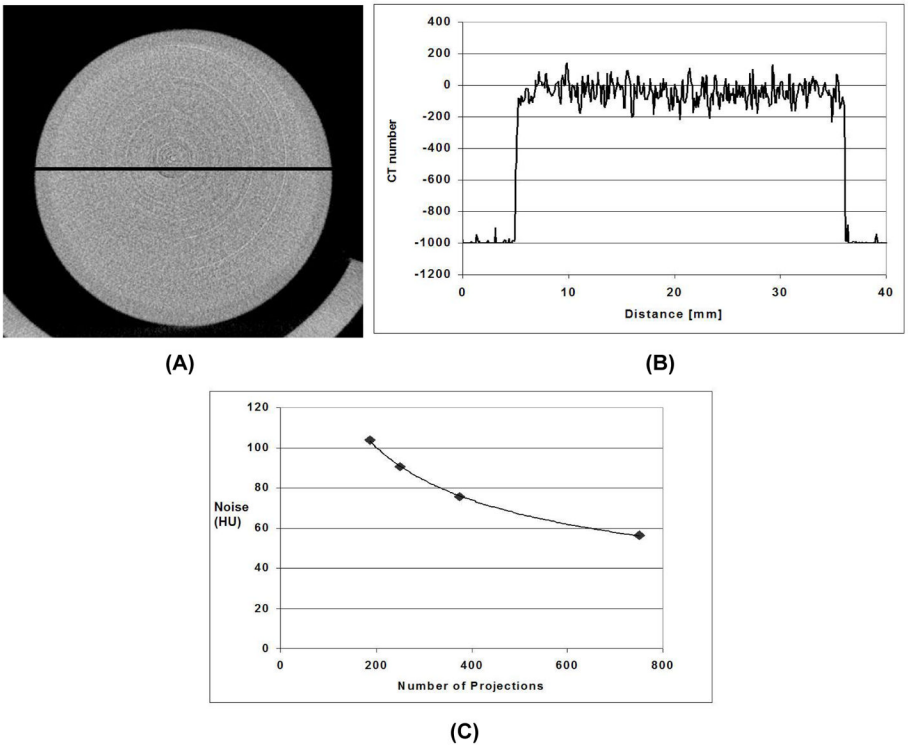

Fig. 4.

(A) Reconstructed axial micro-CT image of a 3 cm diameter water phantom scanned at 80 kVP, 160 mA, 10 ms per exposure and 380 projections showing the line profile that was taken (B). The average level of noise is about 75 HU. The reconstructed voxel is 88^3 microns. The noise as a function of the number of projection images is shown in (C).

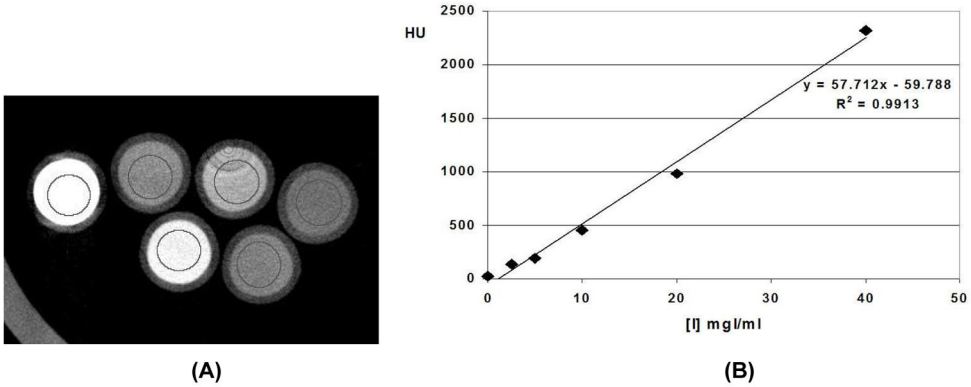

Fig. 5.

(A) Reconstructed axial micro-CT image of a phantom with a water vial and vials with iodine concentration of the following values 2.5, 5, 10, 20, 30 mg I per ml. (B) Linear regression fit of the average signal intensity in ROI in the center of each vial for the 5 different iodine concentration of iodine and water. There is a strong linear correlation between the enhancement (CT number) and the increasing iodine concentration.

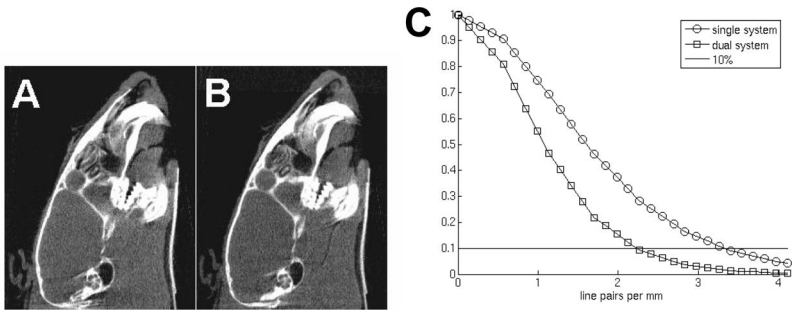

Fig. 6.

(A) A micro-CT slice obtained using a single chain data and (B) the same slice obtained by combining projections obtained with both imaging chains. (C) The MTFs of the single and dual chain micro-CT system measured in reconstructed images as described in ASTM[11].

Fig. 7.
Examples of tomographic slices in three orientations acquired during diastole (A) and systole (B) in a rat using a liposomal blood pool contrast agent.